The effect of cardiac properties on arterial pulse waves: An in–silico study

Francesco Piccioli[1] Alessandro Valiani[1] Jordi Alastruey[2] Valerio Caleffi[1]

August 30, 2022

affiliations: [1]Department of Engineering, University of Ferrara, Via G. Saragat 1, 44122 Ferrara, Italy; [2]School of Biomedical Engineering and Imaging Sciences, King's College London, St Thomas' Hospital, Westminster Bridge Road, London SE1 7EH;

abbreviated title: Cardiac influence on arterial pulse waves

correspondence: Francesco Piccioli, Department of Engineering, University of Ferrara, Via G. Saragat 1, 44122 Ferrara, Italy e-mail: `francesco.piccioli@unife.it`

Abstract

This study investigated the effects of cardiac properties variability on arterial pulse wave morphology using blood flow modelling and pulse wave analysis. A lumped-parameter model of the left part of the heart was coupled to a one-dimensional model of the arterial network and validated using reference pulse waveforms in turn verified by comparison with *in vivo* measurements. A sensitivity analysis was performed to assess the effects of variations in cardiac parameters on central and peripheral pulse waveforms. Results showed that left ventricle contractility, stroke volume, cardiac cycle duration, and heart valves impairment are determinants of central waveforms morphology, pulse pressure and its amplification. Contractility of the left atrium has negligible effects on arterial pulse waves. Results also suggested that it may be possible to infer left ventricular dysfunction by analysing the timing of the dicrotic notch and cardiac function by analysing PPG signals. This study has identified cardiac properties that may be extracted from *in vivo* central and peripheral pulse waves to assess cardiac function.

keywords: Cardiovascular network; Ventricular-arterial coupling; Pulse wave morphology; Sensitivity analysis; Cardiac dysfunction; PPG signal

1 Introduction

Pathologies affecting cardiac function are responsible for morbidity and mortality worldwide[1]. Cardiac haemodynamics properties are of paramount importance for the assessment of cardiac function and, hence, cardiovascular risk. Some cardiac properties are assessed invasively. For example, left ventricular filling pressure – which is used to assess left ventricular function – can be measured directly by placing a catheter in the proximal aorta or the left ventricle, or indirectly from the pulmonary artery[2,3]. This is an expensive and time-consuming procedure that carries risk to patients (e.g., blood clot formation and embolization) due to its invasive nature, even when performed in specialized centres[4].

An indirect estimation of cardiac properties by pulse wave analysis may overcome these obstacles. Currently, pulse wave analysis is usually employed to obtain information on vascular properties, such as arterial stiffness[5], but it has the potential to provide information on cardiac function, since changes in cardiac properties affect the morphology of pulse wave signals measured in the vasculature[6]. Nowadays, pulse waves can be acquired noninvasively by wearable devices which are more convenient and less expensive for large-scale screening than invasive exams. In particular, the photoplethysmogram (PPG) pulse wave is easily acquired using pulse oximeters, which are frequently used in healthcare settings to measure arterial blood oxygen saturation and pulse rate. PPG signals can also be acquired by devices available to the wider population, such as smartwatches and fitness bands[7,8].

Databases of *in silico* pulse waves signals representative of cohorts of real subjects can be produced using robust and efficient computational blood flow models for the development and pre-clinical testing of pulse wave analysis algorithms[9,10]. Virtual subjects are characterised by haemodynamic variables spanning the physiological range, even in disease-related conditions[11,12]. Different numerical models can be employed to accomplish this task: zero-dimensional (0-D) lumped-parameters models for simulating blood flow in distal vessels[13,14,15] and specific organs such as the heart[16], one-dimensional (1-D) models for simulating blood flow in the large arteries of the human circulation[17,18], and three-dimensional (3-D) models[11], whose use is limited to the simulation of blood flow in localised regions of the vasculature due to their high computational cost. 1-D models can simulate pulse wave signals with a reasonable accuracy compared with both 3-D models[19,11] and experimental data[20], and at much lower computational cost compared to 3-D models. They have, therefore, been used to generate databases of pulse waves for thousands of virtual subjects.

The aim of this study is to investigate the effect of cardiac properties on pulse wave morphology using a 1-D model of the arterial vasculature[18] coupled to a 0-D model of cardiac contraction. Previous studies have simulated the ventricular–arterial coupling in 1-D modelling, such as the pioneering work of Formaggia et al.[21], and, more recently, Liang et al.[22], however they aimed to infer the effect of arterial changes caused by ageing on cardiac dynamics. Our 1-D model considers the viscoelastic behaviour of vessel walls[23,24], which is also accounted for in the numerical treatment of boundary conditions[18]. The heart model is based on the state-of-the-art model by Mynard et al.[16,25]. The ability of our model to describe physiological pulse waves for assigned cardiac properties is verified using reference pulse waveforms[25,15]. A sensitivity analysis (SA) is then performed to study the effect of all cardiac model parameters on central and peripheral pulse waveforms, including the PPG

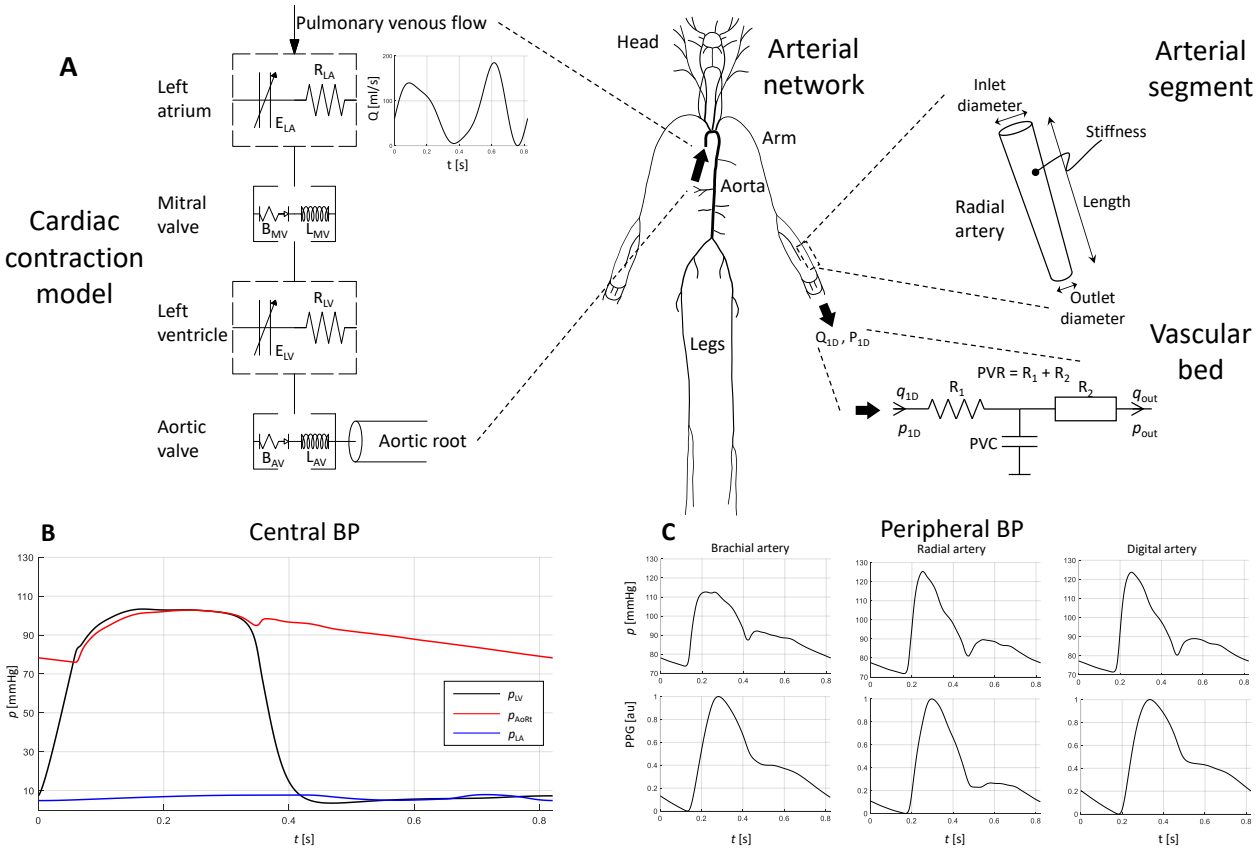

Figure 1: The schematic representation of the 1-D model vascular network coupled with the 0-D cardiac contraction model (A), central blood pressure waveforms (B), peripheral blood pressure waveforms (C). The cardiovascular network consists of the arterial tree, containing the 116 largest systemic arteries, the left-side heart coupled to the vascular network at the aortic root, and lumped parameter models at 1-D model terminal segments representing the vascular bed. See text for the definition of parameters.

signal in the digital artery, so that the perspective of the problem analysed in Formaggia et al.[21] and Liang et al.[22] is reversed.

2 Materials and Methods

2.1 Cardiovascular model

A schematic representation of the proposed cardiovascular model is shown in Fig. 1. It includes three key components. First, the 1-D model arterial network consists of 116 arterial segments representing the largest arteries of the thorax, limbs and head[15]. Arterial segments were modelled as thin viscoelastic tubes of linearly tapered diameter. Second, the RCR Windkessel model was employed at the terminal vessels as outlet boundary condition (BC), to describe the resistance and compliance of peripheral vascular beds. Third, a cardiac contraction model representing the left-side heart was coupled to the vascular network as

inlet BC.

2.1.1 Vascular model

The 1-D model vascular network was modelled using the *augmented fluid-structure interaction (a-FSI) system*[23,24,26], a hyperbolic set of equations. This includes equations for the conservation of mass and momentum, and a closure equation relating vessel cross-sectional area and internal pressure, the so-called tube law[27,23], properly reformulated to take into account the viscoelastic behaviour of vessel walls. Key assumptions for the haemodynamic model are: laminar flow, incompressible and Newtonian fluid (blood density, $\rho = 1060\,\mathrm{kg/m^3}$; blood viscosity, $\mu = 2.5$ mPa s), and no energy losses at bifurcations.

For the geometrical and mechanical characteristics of the network, the reader is referred to Charlton et al.[15]. The viscoelastic formulation of the tube law was described using the Standard Linear Solid Model (SLSM)[28,29], entailing the presence of a *stiff* term in the governing system of equations. Therefore, the numerical scheme was chosen to work efficiently with all ranges of relaxation time. It consists of the stiffly accurate implicit-explicit (IMEX) strong-stability-preserving SSP(3,3,2) scheme, characterised by three stages for both the implicit and explicit parts and second-order accuracy[30,23]. A finite volume (FV) method was used for the discretisation in space. The treatment of internal BCs, i.e. vessel junctions, and external BCs followed the methodology presented by Piccioli et al.[18], which is consistent with the model describing the arterial mechanical behaviour.

2.1.2 Left-side cardiac model

The cardiac contraction model includes the left atrium (LA), the left ventricle (LV), and the adjacent valves, i.e. mitral valve (MV) and aortic valve (AV). The pulmonary venous flow rate (PVFR) entering the LA was prescribed as a function of time. The cardiac contraction model was employed as inlet BC for the vascular model, as described in Sect. 2.1.3.

The LA and LV were modelled through the time-varying elastance function $E(t)$[16]. Mimicking the myocardium contraction, elastance changes between its extrema, relating the pressure in the cavity $p(t)$ with the cavity volume $v(t)$ by

$$p(t) = E(t)\,[v(t) - v_{p0}]\,[1 - K_s\,q_{out}(t)]\,, \tag{2.1}$$

where v_{p0} is the unstressed volume, K_s is a resistive term, and $q_{out}(t)$ is the chamber outflow[16]. The elastance $E(t)$ was defined by the 'double-Hill' function[16,31]

$$E(t) = \left[\frac{E_{max} - E_{min}}{\max(H_1(t)H_2(t))}\right] H_1(t)H_2(t) + E_{min}, \tag{2.2}$$

where E_{min} and E_{max} are the minimal and maximal values of the elastance, respectively. E_{min} governs diastolic passive stiffness, hence the filling phase of the chamber[32], whereas E_{max} is considered to be a measure of systolic contractility[33,34,35]. The functions $H_1(t)$ and $H_2(t)$,

$$H_1(t) = \frac{(\bar{t}/\tau_1)^{m_1}}{1 + (\bar{t}/\tau_1)^{m_1}} \quad \text{and} \quad H_2(t) = \frac{1}{1 + (\bar{t}/\tau_2)^{m_2}}, \tag{2.3}$$

govern the ascending (contraction) and descending (relaxation) tracts of the $E(t)$ curve, respectively, and they were described by shape m_i and time τ_i parameters, with $i = 1, 2$. In Eq. (2.3), $\bar{t}$ is equal to $t - t_{onset}$, with t_{onset} the onset of contraction. The cavity volume $v(t)$ was calculated using the continuity equation

$$\frac{\mathrm{d}v}{\mathrm{d}t} = q_{in}(t) - q_{out}(t), \tag{2.4}$$

where $q_{in}(t)$ and $q_{out}(t)$ are the flow rates entering and leaving the heart chamber.

Valve dynamics, described by the trans-valvular blood flow rate, $q(t)$, and the opening state of the valve, $\zeta(t)$, ranging from 0 to 1, depends on the pressure difference across the valve, $\Delta p(t)$. Valve dynamics over time was expressed via a system of ordinary differential equations (ODE)[16],

$$\frac{\mathrm{d}q}{\mathrm{d}t} = \frac{1}{L(t)} \left[\Delta p(t) - B(t) q(t) \left| q(t) \right| \right], \tag{2.5a}$$

$$\frac{\mathrm{d}\zeta}{\mathrm{d}t} = \mathscr{F}\left(\zeta, K_{vo}, K_{vc}, \Delta p\right) = \begin{cases} \left[1 - \zeta(t)\right] K_{vo}\, \Delta p(t) & \text{if } \Delta p(t) > 0, \\ \zeta(t) K_{vc}\, \Delta p(t) & \text{if } \Delta p(t) < 0, \end{cases} \tag{2.5b}$$

where the coefficients $B(t)$ and $L(t)$ are Bernoulli resistance and blood inertance, respectively. They are expressed as

$$B(t) = \frac{\rho}{2 A_v(t)^2} \quad \text{and} \quad L(t) = \frac{\rho l}{A_v(t)}, \tag{2.6}$$

where $A_v(t)$ is the valve orifice area, and l is the valve length[16]. The orifice area ranges from A_{min} to A_{max} potentially accounting for a leaky or stenotic valve,

$$A_v(t) = \left[A_{max} - A_{min}\right] \zeta(t) + A_{min}. \tag{2.7}$$

The rate of opening or closure of the valve, $\mathrm{d}\zeta/\mathrm{d}t$, depends on the pressure difference, such that when $\Delta p(t)$ is positive the valve opens and the coefficient K_{vo} is employed; otherwise, the valve closes and K_{vc} is used. High values of K_{vo} and K_{vc} indicate a rapid opening and closing of the valve, respectively.

The input to the cardiac contraction model, represented by the pulmonary venous flow rate, was prescribed as a discretised function of time. The PVFR entering the LA accounts for the flow contributions of all the pulmonary veins. It has a double-peaked shape, with two local maxima, i.e. the systolic and diastolic peaks, and two local minima,[16,25,36] as shown in Fig. 1 (A). In this work, PVFR was parametrised using a Fourier function by assigning six parameters: the cardiac cycle duration T, the total volume entering the left atrium in one cardiac cycle, V_{net}, and the four function extrema.

2.1.3 0D-1D coupling

The cardiac contraction model acts as inlet boundary condition to the 1-D model vascular network. The flow rate through the aortic valve, $q_{AV}(t)$, was computed at every time step

and prescribed as the inflow to the aortic root. The coupling between the cardiac model and the arterial domain was accomplished using the following Riemann invariants associated with the genuinely non-linear field at the proximal boundary of the physical domain[18],

$$\Gamma_1 = u - 4c, \quad \Gamma_2 = p - K\left(\sqrt{\alpha} - 1\right), \tag{2.8}$$

where $u(x,t)$ is the cross-sectional averaged blood velocity, $c(x,t)$ is the pulse wave velocity, $p(x,t)$ is the cross-sectional averaged blood pressure (BP), $K(x)$ is the wall stiffness coefficient, and $\alpha = A/A_0$ is the dimensionless luminal cross-sectional area, where $A(x,t)$ and $A_0(x)$ are the time–varying dimensional and equilibrium luminal cross-sectional areas, respectively[23].

In the cardiac contraction model, the time-dependent variables presented in Sect. 2.1.2 must be computed and updated for every time step. These variables are the valve's flow rate, q_v, and state, ζ_v, and the chambers volume, v_c. Subscript c identifies either the LA or the LV, whereas subscript v identifies either the MV or AV. Equations (2.5a) and (2.5b) were integrated in time following the IMEX RK method, treating the equations explicitly since they do not contain *stiff* terms. Thus, the time discretisation of Eq. (2.5a) reads as

$$q_v^{(k)} = q_v^n + \Delta t \sum_{j=1}^{k-1} \tilde{a}_{kj} \left[\frac{1}{L^{(j)}} \left(\Delta p^{(j)} - B^{(j)} q^{(j)} \left| q^{(j)} \right| \right) \right], \tag{2.9a}$$

$$q_v^{n+1} = q_v^n + \Delta t \sum_{k=1}^{s} \tilde{\omega}_k \left[\frac{1}{L^{(k)}} \left(\Delta p^{(k)} - B^{(k)} q^{(k)} \left| q^{(k)} \right| \right) \right]. \tag{2.9b}$$

Here, q_v^n is the flow rate at time t^n, and q_v^{n+1} at $t^{n+1} = t^n + \Delta t$. Matrix $\tilde{\boldsymbol{a}} = (\tilde{a}_{kj})$ is an $s \times s$ matrix characterising the explicit stages of the chosen IMEX RK scheme, while the coefficient vector $\tilde{\boldsymbol{\omega}} = (\tilde{\omega}_1, \ldots, \tilde{\omega}_s)$ represents the explicit weights, with s the number of the Runge-Kutta (RK) stages ($s = 3$ in this work)[37,30]. The same time discretisation scheme was applied to the opening state of the valve to obtain the explicit discretisation of Eq. (2.5b),

$$\zeta_v^{(k)} = \zeta_v^n + \Delta t \sum_{j=1}^{k-1} \tilde{a}_{kj} \, \mathscr{F}\left(\zeta_v^{(j)}, K_{vo,v}^{(j)}, K_{vc,v}^{(j)}, \Delta p_v^{(j)} \right), \tag{2.10a}$$

$$\zeta_v^{n+1} = \zeta_v^n + \Delta t \sum_{k=1}^{s} \tilde{\omega}_k \, \mathscr{F}\left(\zeta_v^{(k)}, K_{vo,v}^{(k)}, K_{vc,v}^{(k)}, \Delta p_v^{(k)} \right). \tag{2.10b}$$

For the mitral valve, Δp_{MV} is the pressure difference between the LA and the LV, whereas, for the aortic valve, Δp_{AV} is the pressure difference between the LV and the first section of the aortic root. Heart chamber pressures were calculated using the stress-strain relationship given by Eq. (2.1). Finally, applying the IMEX RK method to Eq. (2.4), the chamber volume at each RK time step was computed using the inlet and outlet flow rates calculated at the same time step as in Eq. (2.9a), and for the final update those calculated by Eq.

(2.9b), i.e.

$$v_c^{(k)} = v_c^n + \Delta t \sum_{j=1}^{k-1} \tilde{a}_{kj} \left(q_{v,in}^{(j)} - q_{v,out}^{(j)} \right), \tag{2.11a}$$

$$v_c^{n+1} = v_c^n + \Delta t \sum_{k=1}^{s} \tilde{\omega}_k \left(q_{v,in}^{(k)} - q_{v,out}^{(k)} \right). \tag{2.11b}$$

For the LA, $q_{v,in}$ is the pulmonary venous flow rate and $q_{v,out}$ is q_{MV}, whereas for the LV they are q_{MV} and q_{AV}, respectively.

2.2 Sensitivity analysis

Given the wealth of parameters involved in the cardiovascular model, a sensitivity analysis (SA) was performed to identify those parameters that most affect blood pressure waveforms, labelled hereafter as *significant*. Section 2.2.1 presents the cardiovascular parameters varied in the SA, and Section 2.2.2 describes how the significant parameters were identified. Section 2.2.3 introduces the haemodynamic indices studied in the SA.

2.2.1 Model parameters

The parameters defining the cardiovascular model were separated into vascular and cardiac, as indicated in Table 1. The former refer to geometrical and mechanical parameters of the arterial tree, including the RCR parameters of terminal branches. Vascular parameters were taken from Charlton et al.[15]. The cardiac parameters are those of the cardiac contraction model. V_{net} and T were also taken from Charlton et al.[15]. The parameters defining chamber elastance and valve dynamics were set in accordance with Mynard et al.[25]. Their reference values are listed in Appendix A.

The SA focused on the cardiac parameters, since a SA for the vascular parameters was performed by Charlton et al.[15].

2.2.2 Significant parameters evaluation

SA was performed by varying the cardiac parameters listed in Table 1 from their reference values in a univariate manner, i.e. when a parameter is varied, all others remained unchanged. Reference values of heart chamber and valve parameters are listed in Tables 2 and 3, respectively. Variations were performed by increasing and decreasing each reference value by a percentage change that depends on the cardiac parameter considered:

- Cardiac parameters, excluding V_{net}, T, and minimum and maximum valves areas, were varied by $\pm 50\%$ from the reference value. Given the lack of baseline physiological variations of these modelling parameters in the literature, a $\pm 50\%$ was chosen to investigate the effect of these parameters on pulse wave morphology. The resulting variations in LV contractility are generally within the physiological range for different clinical scenarios[38], as shown in Sect. 3.2.2.

– The minimum orifice area of the aortic and mitral valves have a zero reference value, standing for a complete valve closure. Simulations for increased $A_{min,AV}$ and $A_{min,MV}$ were obtained by setting their values to 30 mm^2, corresponding to a severe aortic regurgitant orifice area[39], and to a severe mitral regurgitation[40]. Decreased values have no physical meaning and were not considered. The maximum orifice areas of the aortic and mitral valves, $A_{max,AV}$ and $A_{max,MV}$ respectively, were decreased to simulate severe stenosis scenarios by setting their values to 1 cm^2[41]. Increased values were obtained increasing their reference value by 50%.

– The total volume entering the network in one cardiac cycle, V_{net}, and cardiac cycle duration, T, were varied as described by Charlton et al.[15]. Maximum and minimum values for both parameters were identified in Charlton's database. The positive and negative percentage variations from their reference value were calculated, and the greatest variation in absolute value was used in the SA. As a result, V_{net} varied by ±40%, and T by ±20%. The same percentage changes were used for positive and negative variations to avoid SA asymmetry.

SA simulations were compared in pairs to assess the effect on arterial pressure waveforms of changes in cardiac parameters: (i) *baseline* simulation and (ii) *increased* or *decreased* parameter, respectively. This comparison was made for each parameter at the aortic root, brachial artery, and digital artery. The root mean square deviation (RMSD) was calculated for each pair. RMSDs were found to increase towards the periphery, therefore, the cardiac parameters giving an RMSD in the digital artery above the assigned threshold of 6.5 mmHg were labelled as significant.

2.2.3 Haemodynamic indices

Eleven haemodynamic indices were used in a second SA involving those cardiac parameters identified as significant in Section 2.2.2.

The following four indices of central haemodynamics were considered. Left ventricular contractility, quantified by the contractility index (CI), is the maximum rate of increase in left ventricular pressure during isovolumetric contraction, $\mathrm{d}p_{\mathrm{LV}}/\mathrm{d}t|_{\max}$[38,42]. The rate of increase in flow rate and pressure at the aortic root in early systole, $\Delta q/\Delta t$ and $\Delta p/\Delta t$, respectively. Δq was calculated as the difference between the peak flow rate, $q_{\max}$, and the flow rate at the foot of the waveform, $q_{\min}$, i.e. when the aortic valve opens. Δp is the pulse pressure (PP), i.e. the difference between systolic (SBP) and diastolic (DBP) blood pressures[43]. Δt is the time interval in-between the occurrences of either q_{min} and q_{max} or DBP and SBP. Finally, the maximum rate of decrease of late-systolic flow at the aortic root, $\mathrm{d}q/\mathrm{d}t|_{\mathrm{min,AoRt}}$, as described in Flores Gerónimo et al.[44].

The following four indices of cardiac function were considered: left ventricular ejection time (LVET), stroke volume (SV), left ventricular ejection fraction (EF), and cardiac output (CO). LVET is the time interval between opening and closing of the aortic valve. SV is the difference between simulated left ventricular end-diastolic volume (LVEDV) and end-systolic volume (LVESV). EF is the ratio of SV to LVEDV. Lastly, CO is equal to SV $\times$ 60/T.

The following three vascular indices were considered: PP at a central (aortic root) and peripheral (digital) site, $\mathrm{PP_{AoRt}}$ and $\mathrm{PP_{Di}}$ respectively, and the PP augmentation ratio

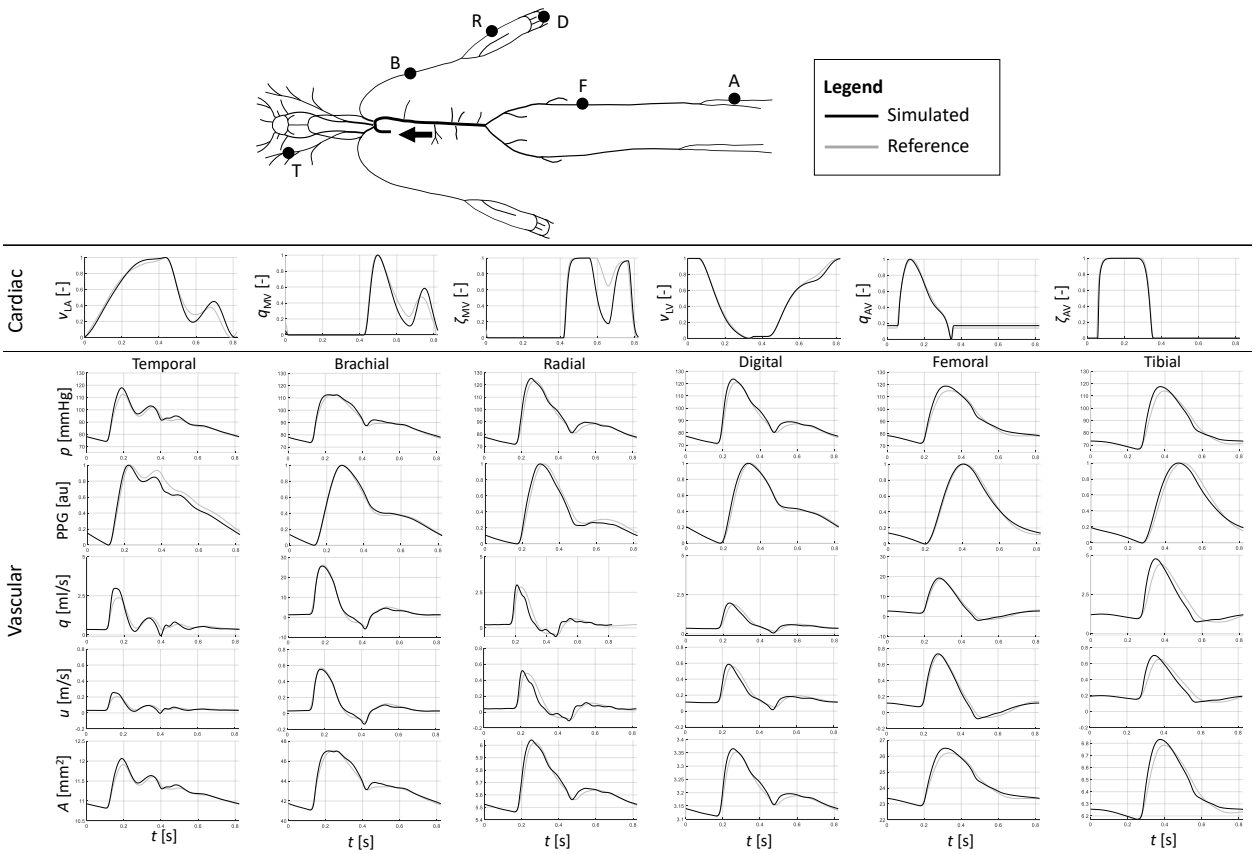

Figure 2: Haemodynamic results of the cardiovascular model. Simulated waveforms are in black solid lines, reference waveforms are in grey solid lines. Cardiac and vascular reference signals were taken from Mynard et al.[25] and Charlton at al.[15], respectively. Cardiac signals are volume in the left atrium (v_{LA}), flow rate through the mitral valve (q_{MV}), state of the mitral valve (ζ_{MV}), volume in the left ventricle (v_{LV}), flow rate through the aortic valve (q_{AV}), state of the aortic valve (ζ_{AV}), normalised to compare reference and simulated signals. Vascular signals are internal pressure (p), PPG signal, flow rate (q), flow velocity (u), and luminal cross-sectional area (A), in the temporal, brachial, radial, digital, femoral, and tibial arteries, as indicated by the labels in the sketch on the top.

200 ($\mathrm{AR_{AoRt-Di}}$) calculated as the percentage increase in PP between the two sites.

3 Results

3.1 Cardiovascular model verification

The vascular network model has been thoroughly tested in previous studies[23,24,18]. Here, we focused on verifying the ability of the cardiac contractility model coupled to the vas-
205 cular network model to produce physiological haemodynamics signals. Figure 2 compares simulated haemodynamics signals with reference *in silico* data, taken from Mynard and Smolich[25], and Charlton et al.[15] in the heart and vasculature, respectively. These reference

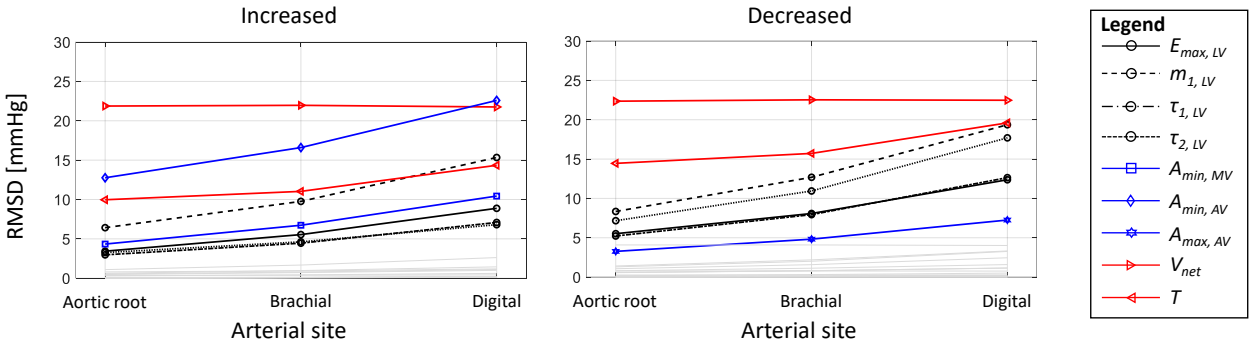

Figure 3: Root mean square deviations (RMSD) computed at the aortic root, brachial and digital arteries for simulations with increased (left) and decreased (right) cardiac parameters values. Significant parameters are divided in parameters of LV contractility (black lines), heart valve-related parameters (blue lines), and V_{net} and T (red lines). Grey lines represent all non-significant parameters.

data were validated against *in vivo* measurements. Since the reference cardiac and vascular models had different cardiac outputs, the cardiac output of the reference vascular model was used to assess the accuracy of our model. Therefore, to qualitatively compare simulated cardiac waveforms with the corresponding reference waveforms, both reference and simulated cardiac signals were normalised. The new model replicated well the morphology of all cardiac signals. The mitral trans-valvular flow rate presents its characteristic double-peaked morphology[45,46], with the E/A ratio equal to 1.7, consistent with literature values[36,25]. Furthermore, the state of the aortic valve variable shows a clear distinction between the LV ejection phase when the valve is open and the LV filling phase when it is closed. These results corroborate the ability of the cardiac contraction model to accurately simulate cardiac haemodynamics.

Figure 2 shows pulse wave signals (flow rate, flow velocity, luminal cross-sectional area, pressure, and PPG, calculated as shown in Appendix C.) at six arterial sites: the temporal artery in the head, three peripheral sites in the arm, namely the brachial, radial, and digital arteries, and two in the leg, the femoral and the anterior tibial arteries. Reference and simulated waveforms are in excellent agreement, with percentage relative RMSDs smaller than 1% for all signals and sites, relative to reference signals.

3.2 Sensitivity analysis

3.2.1 Waveform morphology

RMSDs increased towards the periphery of the vascular network (Fig. 3), where the threshold of significant cardiac parameter was imposed (i.e. at the digital site). The resulting significant cardiac parameters were found to be the same for both scenarios in which cardiac parameters were either increased or decreased from their baseline values. These are parameters mainly attributed to LV contractility: the maximal elastance, $E_{max,LV}$, the contraction shape parameter $m_{1,LV}$, and the contraction and relaxation time parameters, $\tau_{1,LV}$ and $\tau_{2,LV}$, respectively. The other significant parameters were the minimum orifice area of

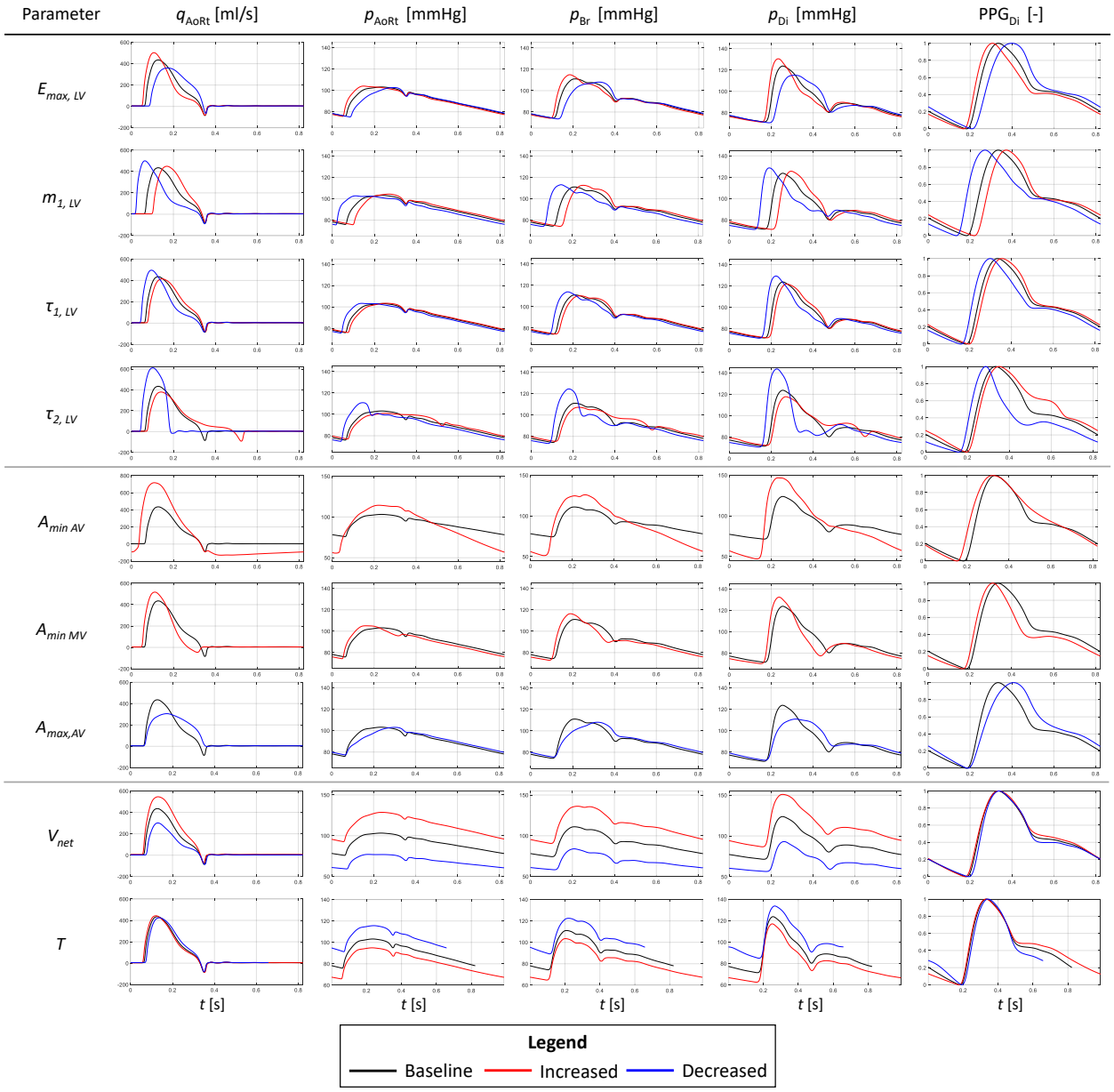

Figure 4: Pulse waveforms at baseline (black), and with increased (red) and decreased (blue) values in the significant cardiac parameters. The following waveforms are shown: flow rate at the aortic root (q_{AoRt}), pressure at the aortic root (p_{AoRt}), pressure in the brachial artery (p_{Br}), and pressure (p_{Di}) and PPG signal ($\mathrm{PPG}_{\mathrm{Di}}$) in the digital artery. Each row represents simulations for a significant cardiac parameter: left ventricular (LV) maximal elastance ($E_{max,LV}$), LV contraction shape parameter ($m_{1,LV}$), LV contraction time parameter ($\tau_{1,LV}$), LV relaxation time parameter ($\tau_{2,LV}$), aortic valve minimum orifice area ($A_{min,AV}$), mitral valve minimum orifice area ($A_{min,MV}$), aortic valve maximum orifice area ($A_{max,AV}$), total volume entering the left atrium in one cardiac cycle (V_{net}), and cardiac cycle duration (T).

the valves, $A_{min,AV}$ and $A_{min,MV}$, the maximum orifice area of the aortic valve, $A_{max,AV}$, in the stenotic scenario, the total volume entering the LA in one cardiac cycle, V_{net}, and

the cardiac cycle duration, T. No cardiac parameters of LA contractility were found to be significant.

Figure 4 shows pulse waveforms both in central and peripheral sites at baseline and with individual variations in the significant cardiac parameters. Changes in wave morphology occurred mainly in systole. LV-related parameters produced minor changes in wave morphology in diastole. The timing of the dicrotic notch only changed when $\tau_{2,LV}$ was varied, since this cardiac parameter regulates the timing of the relaxation phase of LV contractility. With increasing $\tau_{2,LV}$ the relaxation phase of the LV was delayed and, hence, the aortic valve closed later, delaying the time of the dicrotic notch.

Regurgitant valve scenarios show significant variations in pulse wave morphology. With increasing $A_{min,AV}$ the flow rate at the aortic root became negative in diastole due to the reflux caused by the suction effect of the LV during relaxation. Consequently, arterial diastolic pressure decreased. These results suggest that impairment of the AV has direct effects on arterial pulse waves, both at central and peripheral sites. With increasing $A_{min,MV}$ the late-systolic decrease in flow rate occurred more rapidly than in the case of a healthy valve. During LV contraction blood volume was not only ejected in the vascular network through the AV, but part of it is also re-ejected in the LA through the leaking MV. Pressures in the network with regurgitant MV changed less significantly than the AV regurgitation case due to the mitigating function of the LV and the proper action of the AV. Significant variations in wave morphologies were also observed with severe aortic stenosis. With decreased $A_{max,AV}$ the flow rate at the aortic root became more smoothed and with lower peak. In all vascular sites, the rate of increase in early-systolic BP was less steep, with a consequent decrease in PP becoming more evident at the digital site.

Cardiac function, in particular LV contractility, influenced PPG morphology. Variations in PPG signals followed those in digital pressure. Interestingly, in the case of V_{net} variations, PPG pulse waves remained unaltered due to the nearly linear relationship between volume in the network and internal pressure: when only V_{net} varied, the pressure amplitude changed but not the pressure wave morphology.

3.2.2 Haemodynamic indices

Figure 5 summarises the percentage variations in haemodynamic indices with changes in significant cardiac parameters. The reference CI ($\mathrm{d}p_{\mathrm{LV}}/\mathrm{d}t|_{\max}$) was 13.96×10^2 mmHg/s in agreement with literature data[38,42]. The observed variations in CI are consistent with physiologic percentage variations in which CI increased by 133% during exercise and decreased by 47% with cardiomyopathy[38]. Most of the variations reported in Fig. 5 (A) are within this range. CI increased with increasing $E_{max,LV}$ and decreasing $m_{1,LV}$, $\tau_{1,LV}$, and $\tau_{2,LV}$. The most significant variation in CI occurred with the decreasing shape parameter $m_{1,LV}$, which defines the slope of the increasing part of the chamber elastance curve. A smaller $m_{1,LV}$ made the slope steeper raising the rate of increase in p_{LV}. Regurgitant valves and V_{net} caused an increase in CI, whereas T and $A_{max,LV}$ led to negligible effects on CI. $\Delta q/\Delta t$ and $\Delta p/\Delta t$ at the aortic root varied similarly to variations in CI, although at different rates (Fig. 5 (B) and (C)). The variations in $\Delta q/\Delta t$ and $\Delta p/\Delta t$ observed with stenotic aortic valve confirmed the variations in flow rate and BP waveforms observed in Fig. 4. The relation between increased LV contractility and aortic root pulse wave morphology produced by our model is

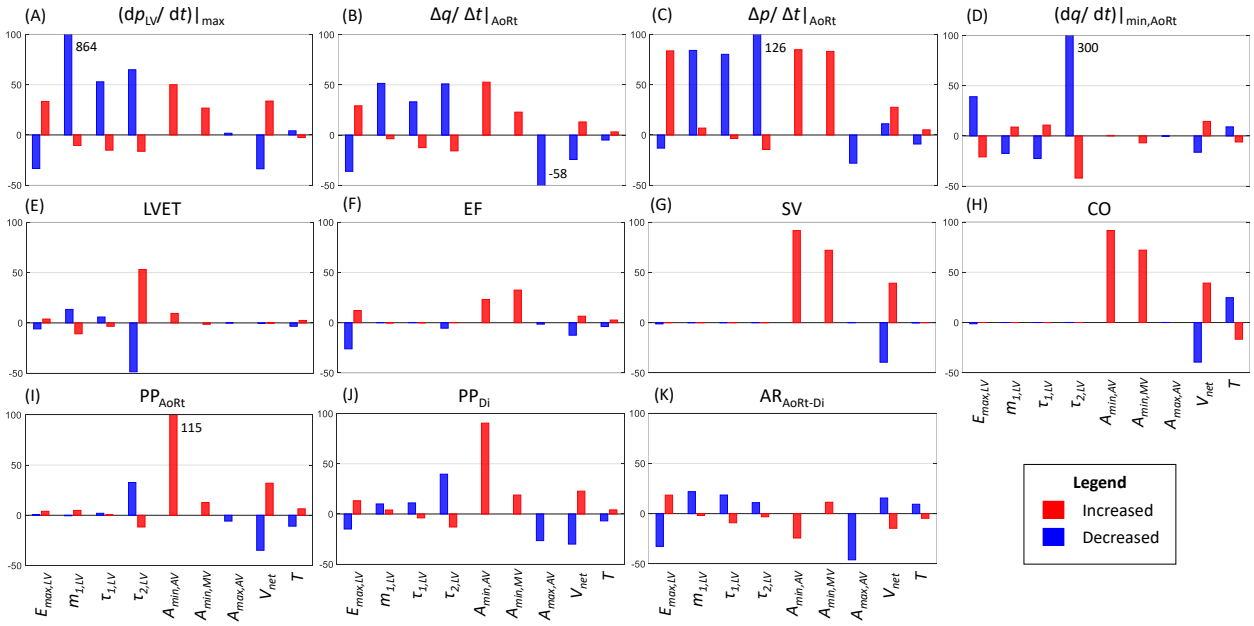

Figure 5: Percentage variations in haemodynamic indices with increased (red) and decreased (blue) values in the significant cardiac parameters. Y-axis show percentage variations in the indices from their corresponding baseline values. Baseline values: contractility index ($dp_{\mathrm{LV}}/dt|_{\mathrm{max}}$), 13.96×10^2 mmHg/s; rate of increase in flow rate in early-systole at the aortic root ($\Delta q/\Delta t|_{\mathrm{AoRt}}$), 6.45×10^3 ml/s^2; rate of increase in pressure in early-systole at the aortic root ($\Delta p/\Delta t|_{\mathrm{AoRt}}$), 1.47×10^2 mmHg/s; maximum rate of decrease of late-systolic flow rate at the aortic root ($dq/dt|_{\mathrm{min,AoRt}}$), 2.42×10^3 ml/s^2; left ventricular ejection time (LVET), 324 ms, ejection fraction (EF), 58 %; stroke volume (SV), 66.4 ml; cardiac output (CO), 4.8 l/min; pulse pressure at the aortic root ($\mathrm{PP_{AoRt}}$), 27.3 mmHg; pulse pressure in the digital artery ($\mathrm{PP_{Di}}$), 52.3 mmHg; and pulse pressure augmentation ratio between the aortic root and the digital artery ($\mathrm{AR_{AoRt-Di}}$), 91.8 %.

consistent with Li et al.[43]. The variations in $\Delta q/\Delta t$ and $\Delta p/\Delta t$ followed the same trend as those in $\mathrm{PP_{Di}}$ (Fig. 5 (J)), in agreement with the morphology of the central pressure wave being a major determinant of peripheral SBP and correlating with the rate of increase in early-systolic aortic flow[43,44]. Moreover, the maximum rate of decrease in late-systolic flow at the aortic root, $dq/dt|_{\mathrm{min,AoRt}}$ in Fig. 5 (D), increased with increasing V_{net}, and decreasing T and LVET, in agreement with Flores Gerónimo et al.[44]

As for LV properties, both EF and LVET were affected by changes in LV contractility, as shown in Fig. 5 (E) and (F). EF also increased with regurgitant valves and increasing V_{net} and T. The variation in LVET became significant when $\tau_{2,LV}$ was varied: it decreased by -48 % with decreasing $\tau_{2,LV}$ and increased by $+52$ % with increasing $\tau_{2,LV}$. This result is consistent with the physical meaning of the contraction and relaxation time parameters. These influence the time of occurrence of the respective sections of the elastance curve: a decrease in $\tau_{1,LV}$ anticipates contraction and an increase in $\tau_{2,LV}$ delays relaxation, and vice-versa. In the case of AV regurgitation, LVET is the time interval when the area of the AV is greater than its minimum value. SV was not affected by the four cardiac parameters

related to LV contractility (Fig. 5 (G)), since V_{net} did not change. A significant increase in SV can be observed with simulated valve regurgitant scenarios, of +92 % and +72 % for the AV and MV, respectively. When the AV does not close completely, part of the volume ejected during the contraction returns into the ventricle during relaxation, as pointed out in Sect. 3.2. This causes both the LV end-diastolic and end-systolic volumes to increase, with a greater increase in the former than the latter, thus resulting in an overall increase in SV. Similarly, the LV ejects blood volume through both valves when the MV is impaired. Thus, the LV end-systolic volume decreases and the end-diastolic volume increases. The stenotic aortic valve scenario did not affect significantly LV end-diastolic and end-systolic volumes, hence, SV did not vary. The aortic stenosis caused a slower ejection of the blood volume, as it is observable from the LV volume trend in the ejection phase, which is not reported here for the sake of brevity. Variations in V_{net} caused SV to change symmetrically from the baseline value, demonstrating that, barring leaking valve scenarios, V_{net} is a surrogate of stroke volume. As expected, CO in Fig. 5 (H) changed consistently with SV and T, most significantly influenced by the former.

The pulse pressure PP showed less variation in central sites compared to the periphery (Fig. 5 (I) and (J)). PP increased with increasing LV contractility, i.e. higher peak and rate of increase in elastance. Both central and peripheral PP increased with shortened LVET, observable from variations in $\tau_{2,LV}$. Regurgitant valves and increased V_{net} and T also raised PP, which instead decreased with severe aortic stenosis. Greater contractility augmented $\mathrm{AR_{AoRt-Di}}$ (Fig. 5 (K)), hence enhancing the physiological effect of PP amplification towards peripheral sites[15,43]. $\mathrm{AR_{AoRt-Di}}$ decreased with regurgitant AV, caused by the greater increase in $\mathrm{PP_{AoRt}}$ compared to $\mathrm{PP_{Di}}$ from their baseline values.

4 Discussion

This work has studied the relationship between cardiac properties and vascular haemodynamics using a state-of-the-art 0-D model properly coupled to a vascular 1-D model by treating the 0-D model with the IMEX-RK SSP scheme for the time discretisation, consistently with the 1-D model. It has been demonstrated that the presented cardiovascular model correctly reproduces human haemodynamics, consistent with *in vivo* measurements. The sensitivity analysis has shown that variations in cardiac properties are associated with identifiable variations in waveform morphology, suggesting the possibility of applying techniques for inverse problem solving, going from a specific pressure waveform to the changes in cardiac characteristics that generated it. Moreover, LA contractility has negligible effects on vascular pulse waves, suggesting that LA properties can not be derived from a pulse wave analysis. At baseline values, $E_{max,LA}$ is equal to 0.13 mmHg/ml, whereas $E_{max,LV}$ is equal to 2.8 mmHg/ml, producing peak LA and LV pressures of 8 mmHg and 103 mmHg, respectively. Thus, even the variations in LA contractility parameters fail to produce significant changes in LA pressure sufficient to affect vascular haemodynamics. In contrast, LV contractility, stroke volume, cardiac cycle duration, and impaired valves function have a considerable influence on arterial pulse waves, being determinants of central waveforms morphology, pulse pressure and its amplification. The greatest variations in PP were found at peripheral sites rather than central sites, which may be more valuable sites for extracting

information about cardiac function by pulse wave analysis. Furthermore, our results have corroborated the findings of previous studies showing strong correlations between LV contractility, aortic blood flow and PP[44,43,47], and the crucial role of cardiac function in both central and peripheral pressure amplitudes[1,48].

Our results have shown that LV contractility, measured by CI, is related to peak elastance, $E_{max,LV}$, rate of LV contraction, and LVET. An increase in $E_{max,LV}$ allows the LV pressure to reach higher values, as $E_{max,LV}$ and LV pressure are directly related through the strain-stress relationship of the cardiac chamber. CI increases with a faster contraction simulated by decreased $m_{1,LV}$, and time parameters. As $\tau_{1,LV}$ decreases, LV pressure increases more rapidly, and so does pressure and flow rate at the aortic root. Moreover, the decrease in $\tau_{2,LV}$ results in a shortening of LVET, leading to the same SV being ejected in a shorter time inteval, making the ejection more impulsive. The increase in contractility correlates with the increase in the PP augmentation ratio, i.e. PP increases more in the periphery than centrally (Fig. 5 (A) and (K)). Furthermore, increased CI is associated with greater SBP peaks in the waveforms (see Fig. 4). This phenomenon is generally more pronounced towards the periphery, and is evident in the case of decreased $\tau_{2,LV}$. The total blood volume entering the network in one cardiac cycle, V_{net}, and cardiac cycle duration, T, both affected blood pressure in the vascular network. With increasing V_{net} and T, PP increased at both the central and peripheral sites, but the PP augmentation ratio decreased from the baseline simulation. Results have shown that valve impairment affects pulse waves, particularly in the case of a regurgitant and stenotic AV due to its direct coupling with the vascular network. With aortic regurgitation, central PP increased more than peripheral PP due to the increased SV. Central arteries have greater compliance than peripheral ones, hence they undergo a greater cross-sectional area dilation and, so, greater increase in PP. With aortic stenosis there is no variation in SV and PP changes more significantly in the peripheral site. Further research is needed to investigate the correlation between valve disease and peripheral pressure in a large cohort of *in vivo* subjects with valve dysfunction via non-invasive measurements of peripheral BP.

Some aspects of our cardiovascular model should be underlined. Firstly, some cardiac parameters that characterise the LV contractility and describe the elastance function cannot be measured directly. Therefore, it is cumbersome to define a physiological range of values for these parameters. Secondly, cardiac parameters affect vascular haemodynamics independently of each other, enabling the study of the effect on pulse wave morphology of independent changes in cardiac properties. This is not the case *in vivo*, where it would be challenging to change LV contractility, for example through pharmacological intervention, without affecting the properties of the vasculature, and vice-versa. Finally, an open–loop model has been used and, thus, some parameters must be imposed, e.g. V_{net}, de facto imposing the venous return. This is numerically implemented through the parametrisation of the pulmonary venous flow rate entering the LA. Physiologically, an impaired LV function can affect the venous return, but this cause–effect phenomenon cannot be regarded in an open–loop cardiovascular model. To overcome this limitation, a decreased venous return is included in the SA through a variation in V_{net}. Therefore, the open–loop model does not weaken the results presented. The implementation of a closed–loop will be object of future work.

This work suggests that it may be possible to infer LV dysfunction, such as an impaired

relaxation phase, by analysing the timing of the dicrotic notch. Results show that the time of diastole of the pulse waveform only varies with the relaxation time parameter of the LV elastance function, but is not affected by other cardiac parameters. This study also offers valuable insight into in the field of hypertension. Lately, the importance of LV contractility in hypertension has been studied, showing that LV function is a major determinant of blood pressure elevation[1,48,49,44,43]. Our results support this thesis, as PP increased with increasing LV contractility without changes in vascular properties. Moreover, hypertension has been found to be related to left ventricular hypertrophy, a response to chronic pressure overload[50], and heart valves disease[51,52,53]. Assessing cardiac properties by arterial pulse wave analysis may allow cardiac function characterisation without the need for invasive catheterization. Results have shown that alterations in blood pressure waves amplify towards the periphery of the systemic circulation (see the RMSDs trends and variations in PP_{Di} and $AR_{AoRt-Di}$ when significant cardiac parameters were varied). Therefore, easily accessible measurements in peripheral arteries could be employed, such as in the radial artery, or one of its surrogates, the digital artery[54].

Finally, our results have highlighted the importance of studying PPG signals, as already presented in previous works in which machine learning models were employed to determine haemodynamic properties using pulse waves and PPG data[8,7]. Such models could also be applied to infer cardiac properties from peripheral pressure measurements and PPG signals. Given the popularity of wearable devices, such as FitBits, smartwatches and oxymetries that are able to measure PPG signals, understanding their correlation with cardiac function could provide consumers with personal tools for monitoring cardiac function.

5 Conclusions

We have presented a theoretical, computationally-based study to arouse interest in assessing cardiac function from arterial pressure waves and peripheral PPG signals. We have validated an open–loop cardiovascular model accounting for ventricular–aortic coupling by showing its ability to simulate accurately cardiac and vascular haemodynamics when compared with reference models validated using *in vivo* measurements.

Results from this model suggest that cardiac parameters related to LV contraction and systolic ejection can be identified by pulse wave analysis. Altered contractility affects aortic flow rate and pressure waveforms, which in turn affect pulse pressure in central and peripheral sites. An impaired LV relaxation phase can be identified from the analysis of the dicrotic notch timing. Moreover, stenotic and regurgitant valves affect the flow rate at the aortic root and pressure waveforms throughout the vasculature. Pulse pressure was found to increase with aortic regurgitation, and to decrease with aortic stenosis. We have demonstrated that an altered venous return in the left atrium affects LV contractility and arterial pulse pressures. In addition, the variations in pulse waves caused by changes in cardiac function were found to amplify towards the periphery of the systemic vasculature, suggesting the suitability of peripheral sites (e.g., radial and digital arteries) for assessing cardiac function. Finally, we have found PPG signals in the periphery to vary with changes in cardiac parameters and diseased valves, suggesting that further work on the analysis of peripheral PPG signals could improve cardiac dysfunction detection from easily–accessible pulse waves measurements.

Conflict of Interest

No conflict of interest.

Acknowledgements

AV was funded by FIR 2020 of the University of Ferrara. VC was funded by MIUR FFABR 2017. JA acknowledges support from the EPSRC [EP/K031546/1], the Wellcome/EPSRC Centre for Medical Engineering at King's College London [WT 203148/Z/16/Z], the Department of Health through the National Institute for Health Research (NIHR) Cardiovascular MedTech Co-operative at Guy's and St Thomas' NHS Foundation Trust (GSTT), and the comprehensive Biomedical Research Centre and Clinical Research Facilities awards to Guy's and St Thomas' NHS Foundation Trust in partnership with King's College London and King's College Hospital NHS Foundation Trust.

Ethical Statement

No experimentation occurred on human or animal subjects for this work.

A Sensitivity Analysis: reference parameters

Reference values for V_{net} and T were 66.3 ml and 0.822 s, respectively[15]. Tables 2 and 3 show the reference cardiac parameters[25] that were increased by + 50 % and decreased by − 50 % in the sensitivity analysis.

B Sensitivity Analysis: RMSD

Table 4 shows the RMSD evaluated in the three sites of analysis in the network, i.e. the aortic root (AoRt), the brachial artery (Br), and the digital artery (Di). Results are reported for each cardiac parameter and for both variations, i.e ± 50 %.

C Simulation of PPG signals

The PPG is conceived as a measurement of volumetric change of arterial blood in a tissue[15,6]. From an operational standpoint, PPG signals were calculated as described next, depending on the site of analysis:

– At the periphery (e.g. the digital artery), the PPG was calculated from the volume of blood stored in the terminal Windkessel model:

$$PPG(t) = \int_0^t q_{1D}(t') - q_{out}(t')\mathrm{d}t', \tag{C.1}$$

where q_{1D} is the inflow to the terminal Windkessel, and q_{out} is the outflow, as shown in Fig. 1.

– At distal sites within the arterial network (e.g. the wrist), the PPG was computed by assuming that the volume of blood in the local microvasculature can be modelled by a Windkessel model. The validity of this assumption relies on the fact that vascular beds at sites within the arterial network are perfused by arterioles branching from the major artery at that site (e.g. the radial artery at the wrist), which are too small to be represented in the arterial network using 1-D modelling. Hence, the inflow to the Windkessel model was assumed to be proportional to the flow in the arterial segment, at a pressure equal to that of the arterial segment. The PPG was calculated using Eq. (C.1), where q_{1D} was set equal to the flow through the arterial segment, and q_{out} was calculated using

$$q_{out}(t) = \frac{p_{1D}(t) - p_{out}}{R}, \tag{C.2}$$

where

$$R = \frac{\langle p_{1D}(t)\rangle - p_{out}}{\langle q_{1D}(t)\rangle}, \tag{C.3}$$

and p_{out} is the outflow pressure, with $\langle p_{1D}\rangle$ and $\langle q_{1D}\rangle$ the blood pressure and flow rate, respectively, obtained at the site of measurement and averaged over the cardiac cycle.

In both cases, the PPG was finally obtained by normalising the pulsatile variation in blood volume within the range $[0, 1]$.

References

1. Gaddum N, Alastruey J, Chowienczyk P, Rutten MC, Segers P, Schaeffter T. Relative contributions from the ventricle and arterial tree to arterial pressure and its amplification: An experimental study. *American Journal of Physiology - Heart and Circulatory Physiology* 2017; 313(3): H558–H567. doi: 10.1152/ajpheart.00844.2016

2. Sharma GV, Woods PA, Lambrew CT, et al. Evaluation of a noninvasive system for determining left ventricular filling pressure. *Archives of Internal Medicine* 2002; 162(18): 2084–2088. doi: 10.1001/archinte.162.18.2084

3. Reddy YN, Nishimura RA. *Hemodynamics for the structural interventionalist*. Philadelphia: Elsevier. 2021

4. McEniery CM, Cockcroft JR, Roman MJ, Franklin SS, Wilkinson IB. Central blood pressure: Current evidence and clinical importance. *European Heart Journal* 2014; 35(26): 1719–1725. doi: 10.1093/eurheartj/eht565

5. Mynard JP, Kondiboyina A, Kowalski R, Cheung MMH, Smolich JJ. Measurement , Analysis and Interpretation of Pressure / Flow Waves in Blood Vessels. *Frontiers in Physiology* 2020. doi: 10.3389/fphys.2020.01085

6. Huttunen JM, Kärkkäinen L, Honkala M, Lindholm H. Deep learning for prediction of cardiac indices from photoplethysmographic waveform: A virtual database approach. *International Journal for Numerical Methods in Biomedical Engineering* 2020; 36(3): 1–17. doi: 10.1002/cnm.3303

7. Wang T, Jin W, Liang F, Alastruey J. Machine learning-based pulse wave analysis for early detection of abdominal aortic aneurysms using in silico pulse waves. *Symmetry* 2021; 13(5). doi: 10.3390/sym13050804

8. Elgendi M. *PPG Signal Analysis: An Introduction Using MATLAB*. Boca Raton: CRC Press. first edit ed. 2020

9. Ambrosi D, Quarteroni A, Rozza G. *Modeling of Physiological Flows*. Springer. 2012

10. Willemet M, Vennin S, Alastruey J. Computational assessment of hemodynamics-based diagnostic tools using a database of virtual subjects: Application to three case studies. *Journal of Biomechanics* 2016; 49(16): 3908–3914. doi: 10.1016/j.jbiomech.2016.11.001

11. Jin W, Alastruey J. Arterial pulse wave propagation across stenoses and aneurysms: Assessment of one-dimensional simulations against three-dimensional simulations and in vitro measurements. *Journal of the Royal Society Interface* 2021; 18(177). doi: 10.1098/rsif.2020.0881

12. Reymond P, Merenda F, Perren F, Rüfenacht D, Stergiopulos N. Validation of a one-dimensional model of the systemic arterial tree. *American Journal of Physiology - Heart and Circulatory Physiology* 2009; 297(1): 208–222. doi: 10.1152/ajpheart.00037.2009

13. Maastricht University, Department of Biomedical Engineering. Circadapt Model.

14. Le Gall A, Vallée F, Pushparajah K, et al. Monitoring of cardiovascular physiology augmented by a patient-specific biomechanical model during general anesthesia. A proof of concept study. *PLoS ONE* 2020; 15(5): 1–19. doi: 10.1371/journal.pone.0232830

15. Charlton PH, Mariscal Harana J, Vennin S, Li Y, Chowienczyk P, Alastruey J. Modeling arterial pulse waves in healthy aging: a database for in silico evaluation of hemodynamics and pulse wave indexes. *American Journal of Physiology. Heart and Circulatory Physiology* 2019; 317(5): H1062–H1085. doi: 10.1152/ajpheart.00218.2019

16. Mynard JP. *Computer modeling and wave intensity analysis of perinatal cardiovacular fucntion and dysfunction*. PhD thesis. University of Melbourne, 2011.

17. Müller LO, Blanco PJ, Watanabe SM, Feijóo RA. A high-order local time stepping finite volume solver for one-dimensional blood flow simulations: application to the ADAN model. *International Journal for Numerical Methods in Biomedical Engineering* 2016; 32(10): e02761. doi: 10.1002/cnm.2761

18. Piccioli F, Bertaglia G, Valiani A, Caleffi V. Modeling blood flow in networks of viscoelastic vessels with the 1D augmented fluid-structure interaction system. *Journal of Computational Physics* 2022; 464: 111364. doi: 10.1016/j.jcp.2022.111364

19. Xiao N, Alastruey J, Figueroa CA. A systematic comparison between 1-D and 3-D hemodynamics in compliant arterial models. *International Journal for Numerical Methods in Biomedical Engineering* 2014; 30(2): 204–231. doi: 10.1002/cnm.2598

20. Matthys KS, Alastruey J, Peiró J, et al. Pulse wave propagation in a model human arterial network: Assessment of 1-D numerical simulations against in vitro measurements. *Journal of Biomechanics* 2007; 40(15): 3476–3486. doi: 10.1016/j.jbiomech.2007.05.027

21. Formaggia L, Lamponi D, Tuveri M, Veneziani A. Numerical modeling of 1D arterial networks coupled with a lumped parameters description of the heart. *Computer Methods in Biomechanics and Biomedical Engineering* 2006; 9(5): 273–288. doi: 10.1080/10255840600857767

22. Liang FY, Takagi S, Himeno R, Liu H. Biomechanical characterization of ventricular–arterial coupling during aging: A multi-scale model study. *Journal of Biomechanics* 2009; 42(6): 692–704. doi: 10.1016/j.jbiomech.2009.01.010

23. Bertaglia G, Caleffi V, Valiani A. Modeling blood flow in viscoelastic vessels: the 1D augmented fluid–structure interaction system. *Computer Methods in Applied Mechanics and Engineering* 2020; 360: 112772. doi: 10.1016/j.cma.2019.112772

24. Bertaglia G, Navas-Montilla A, Valiani A, Monge García MI, Murillo J, Caleffi V. Computational hemodynamics in arteries with the one-dimensional augmented fluid-structure interaction system: viscoelastic parameters estimation and comparison with in-vivo data. *Journal of Biomechanics* 2020; 100: 109595. doi: 10.1016/j.jbiomech.2019.109595

25. Mynard JP, Smolich JJ. One-Dimensional Haemodynamic Modeling and Wave Dynamics in the Entire Adult Circulation. *Annals of Biomedical Engineering* 2015; 43(6): 1443–1460. doi: 10.1007/s10439-015-1313-8

26. Bertaglia G, Caleffi V, Pareschi L, Valiani A. Uncertainty quantification of viscoelastic parameters in arterial hemodynamics with the a-FSI blood flow model. *Journal of Computational Physics* 2021; 430: 110102. doi: 10.1016/j.jcp.2020.110102

27. Bertaglia G, Ioriatti M, Valiani A, Dumbser M, Caleffi V. Numerical methods for hydraulic transients in visco-elastic pipes. *Journal of Fluids and Structures* 2018; 81: 230–254. doi: 10.1016/j.jfluidstructs.2018.05.004

28. Lakes R. *Viscoelastic Materials*. Cambridge University Press. 2009

29. Gutierrez-Lemini D. *Engineering Viscoelasticity*. Springer. 2014

30. Pareschi L, Russo G. Implicit-explicit Runge-Kutta schemes and applications to hyperbolic systems with relaxation. *Journal of Scientific Computing* 2005; 25(1): 129–155. doi: 10.1007/s10915-004-4636-4

31. Maksuti E, Westerhof N, Westerhof BE, Broomé M, Stergiopulos N. Contribution of the arterial system and the heart to blood pressure during normal aging - A simulation study. *PLoS ONE* 2016; 11(6): 1–12. doi: 10.1371/journal.pone.0157493

32. Stergiopulos N, Meister JJ, Westerhof N. Determinants of stroke volume and systolic and diastolic aortic pressure. *American Journal of Physiology - Heart and Circulatory Physiology* 1996; 270(6 39-6): H2050–H2059. doi: 10.1152/ajpheart.1996.270.6.h2050

33. Segers P, Stergiopulos N, Westerhof N. Quantification of the contribution of cardiac and arterial remodeling to hypertension. *Hypertension* 2000; 36(5): 760–765. doi: 10.1161/01.HYP.36.5.760

34. Mynard JP, Smolich JJ, Davidson MR, Penny D. A simple, versatile valve model for use in lumped parameter and one-dimensional cardiovascular models. *International Journal for Numerical Methods in Biomedical Engineering* 2011; 28(6-7): :626–41. doi: 10.1002/cnm

35. Simakov SS. Lumped parameter heart model with valve dynamics. *Russian Journal of Numerical Analysis and Mathematical Modelling* 2019; 34(5): 289–300. doi: 10.1515/rnam-2019-0025

36. Sun Y, Sjoberg BJ, Ask P, Loyd D, Wranne B. Mathematical model that characterizes transmitral and pulmonary venous flow velocity patterns. *American Journal of Physiology - Heart and Circulatory Physiology* 1995; 268(1 37-1). doi: 10.1152/ajpheart.1995.268.1.h476

37. Pareschi L, Russo G. Implicit-explicit Runge-Kutta schemes for stiff systems of differential equations. *Recent Trends in Numerical Analysis* 2001; 3(5): 269–288.

38. Mynard JP, Nithiarasu P. A 1D arterial blood flow model incorporating ventricular pressure, aortic valve and regional coronary flow using the locally conservative Galerkin (LCG) method. *Communication in Numerical Methods in Engineering* 2008; 24(5): 367–417. doi: 10.1002/cnm.1117

39. Steeds RP, Myerson SG. Imaging assessment of mitral and aortic regurgitation: current state of the art. *Heart (British Cardiac Society)* 2020; 106(22): 1769–1776. doi: 10.1136/heartjnl-2019-316216

40. Carabello BA. Progress in mitral and aortic regurgitation. *Progress in Cardiovascular Diseases* 2001; 43(6): 457–475. doi: 10.1053/pcad.2001.24597

41. Baumgartner H, Hung J, Bermejo J, et al. Echocardiographic assessment of valve stenosis: EAE/ASE recommendations for clinical practice. *European Journal of Echocardiography* 2009; 10(1): 1–25. doi: 10.1093/ejechocard/jen303

42. Chengode S. Left ventricular global systolic function assessment by echocardiography. *Annals of Cardiac Anaesthesia* 2016; 19(5): S26–S34. doi: 10.4103/0971-9784.192617

43. Li Y, Guilcher A, Charlton PH, Vennin S, Alastruey J, Chowienczyk P. Relationship between fiducial points on the peripheral and central blood pressure waveforms: rate of rise of the central waveform is a determinant of peripheral systolic blood pressure. *American Journal of Physiology. Heart and Circulatory Physiology* 2021; 320(4): H1601–H1608. doi: 10.1152/ajpheart.00818.2020

44. Flores Gerónimo J, Corvera Poiré E, Chowienczyk P, Alastruey J. Estimating Central Pulse Pressure From Blood Flow by Identifying the Main Physical Determinants of Pulse Pressure Amplification. *Frontiers in Physiology* 2021; 12 (February): 1–15. doi: 10.3389/fphys.2021.608098

45. Luisada AA, Watanabe K, Bhat PK, Rao DB, Knighten V. Correlates of the Echocardiographic Waves of the Mitral Valve in Normal Subjects of Various Ages. *Journal of the American Geriatrics Society* 1975; 23(5): 216–223. doi: 10.1111/j.1532-5415.1975.tb00188.x

46. Seo JH, Mittal R. Effect of diastolic flow patterns on the function of the left ventricle. *Physics of Fluids* 2013; 25(11). doi: 10.1063/1.4819067

47. Pagoulatou S, Adamopoulos D, Rovas G, Bikia V, Stergiopulos N. The effect of left ventricular contractility on arterial hemodynamics: A model-based investigation. *PLoS ONE* 2021; 16: 1–14. doi: 10.1371/journal.pone.0255561

48. Vennin S, Li Y, Willemet M, et al. Identifying hemodynamic determinants of pulse pressure: A combined numerical and physiological approach. *Hypertension* 2017; 70(6): 1176–1182. doi: 10.1161/HYPERTENSIONAHA.117.09706

49. Li Y, Gu H, Fok H, Alastruey J, Chowienczyk P. Forward and Backward Pressure Waveform Morphology in Hypertension. *Hypertension* 2017; 69(2): 375–381. doi: 10.1161/HYPERTENSIONAHA.116.08089

50. Segers P, Stergiopulos N, Schreuder JJ, Westerhof BE, Westerhof N. Left ventricular wall stress normalization in chronic pressure-overloaded heart: A mathematical model study. *American Journal of Physiology - Heart and Circulatory Physiology* 2000; 279(3 48-3): 1120–1127. doi: 10.1152/ajpheart.2000.279.3.h1120

51. Pai RG, Varadarajan P. Prognostic implications of mitral regurgitation in patients with severe aortic regurgitation. *Circulation* 2010; 122(11 SUPPL. 1): 43–47. doi: 10.1161/CIRCULATIONAHA.109.927921

52. Bonow RO. Chronic mitral regurgitation and aortic regurgitation: Have indications for surgery changed?. *Journal of the American College of Cardiology* 2013; 61(7): 693–701. doi: 10.1016/j.jacc.2012.08.1025

53. Mrsic Z, Hopkins SP, Antevil JL, Mullenix PS. Valvular Heart Disease. *Primary Care - Clinics in Office Practice* 2018; 45(1): 81–94. doi: 10.1016/j.pop.2017.10.002

54. Millasseau SC, Guigui FG, Kelly RP, et al. Noninvasive assessment of the digital volume pulse: Comparison with the peripheral pressure pulse. *Hypertension* 2000; 36(6): 952–956. doi: 10.1161/01.HYP.36.6.952

Table 1: Vascular (VV) and cardiac (CC) parameters of the numerical model. VV parameters: vessel length (L), proximal and distal vessel radius (r_{in} and r_{out}, resp.), vessel stiffness ($E_Y h$, where E_Y is the Young's modulus and h is vessel thickness) computed via Eq. (2) in[15], reference pressure (p_{ref}), RCR outlet pressure (p_{out}), and RCR resistances and compliance (R_1, R_2, C, resp.). CC parameters: total volume entering the LA in one cardiac cycle (V_{net}), cardiac cycle duration (T), minimal and maximal elastance (E_{min} and E_{max}, resp.), shape and time parameters ($m_{1,2}$ and $\tau_{1,2}$, resp.), source resistance (K_s), unstressed and initial volumes (v_{p0} and v_0, resp.) and onset time of the elastance function (t_{onset}); minimum and maximum valve orifice areas (A_{min} and A_{max}, resp.), valve opening and closure constants (K_{vo} and K_{vc}, resp.), and valve length (l). Subscripts c and v refer to chamber and valve, respectively.

VV	L [m] p_{out} [Pa]	r_{in}, r_{out} [m] R_1 [Pa s/m^3]	$E_Y h$ [Pa m] R_2 [Pa s/m^3]	p_{ref} [Pa] C [m^3/Pa]	p_{ext} [Pa]
CC	V_{net} [m^3] T [s] $A_{min,v}$ [m^2] $A_{max,v}$ [m^2]	$E_{min,c}$ [Pa/m^3] $E_{max,c}$ [Pa/m^3] $K_{vo,v}$ [1/Pa s] $K_{vc,v}$ [1/Pa s]	$m_{1,c}$ [-], $\tau_{1,c}$ [s] $m_{2,c}$ [-], $\tau_{2,c}$ [s] l_v [m]	$v_{p0,c}$ [m^3] $v_{0,c}$ [m^3]	$K_{s,c}$ [s/m^3] $t_{onset,c}$ [s]

Table 2: Reference parameters of the cardiac contraction model for the heart chambers: left atrium (LA) and left ventricle (LV). The references values of the heart chambers were taken from Mynard et al.[25].

Chamber	E_{min} [$\frac{\text{Pa}}{\text{cm}^3}$]	E_{max} [$\frac{\text{Pa}}{\text{cm}^3}$]	K_S [$\frac{\text{s}}{\text{cm}^3}$]	v_{p0} [cm^3]	v_0 [cm^3]	m_1 [-]	τ_1 [s]	m_2 [-]	τ_2 [s]	t_{onset} [s]
LA	12.0	17.3	250	3.00	7.10	1.99	0.042	11.2	0.138	0.00
LV	9.33	373	500	1.00	136	1.32	0.215	21.9	0.362	0.65

Table 3: Reference parameters of the cardiac contraction model for the heart valves: mitral valve (MV) and aortic valve (AV). The reference A_{min} is equal to zero for both valves. The references values for valves dynamics were taken from Mynard et al.[25].

Valve	A_{max} [cm^2]	l [cm]	K_{vo} [Pa^{-1}s^{-1}]	K_{vo} [Pa^{-1}s^{-1}]
MV	5.1	2.0	0.2	0.4
AV	4.9	1.0	0.2	0.2

Table 4: Root mean square deviations (RMSD) in mmHg from the sensitivity analysis performed in an univariate manner. The *Increased* and *Decreased* columns stand for the simulations with the increased or decreased cardiac parameter, respectively. The amount of variation for each parameter is addressed in Sect 2.2.2. Cardiac parameters are classified per cardiac site, namely left ventricle (LV), left atrium (LA), aortic valve (AV), and mitral valve (MV). The total volume entering the LA in a cardiac cycle, V_{net}, and the cardiac cycle duration T are not attributed to any cardiac site because they describe overall cardiac function. Significant parameters are reported in bold.

Cardiac site	Param.	Increased			Decreased		
		AoRt	*Br*	*Di*	*AoRt*	*Br*	*Di*
–	$\boldsymbol{V_{net}}$	**21.9**	**22.0**	**21.8**	**22.4**	**22.5**	**22.5**
	$\boldsymbol{T}$	**10.0**	**11.0**	**14.3**	**14.5**	**15.7**	**19.6**
LV	$\boldsymbol{E_{max}}$	**3.43**	**5.54**	**8.88**	**5.51**	**8.08**	**12.4**
	E_{min}	0.80	0.92	1.19	0.58	0.82	1.14
	$\boldsymbol{m_1}$	**6.42**	**9.76**	**15.3**	**8.34**	**12.7**	**19.4**
	$\boldsymbol{\tau_1}$	**2.97**	**4.45**	**7.08**	**5.22**	**7.94**	**12.6**
	m_2	0.63	0.97	1.44	1.41	2.19	3.32
	$\boldsymbol{\tau_2}$	**3.26**	**4.62**	**6.80**	**7.17**	**10.9**	**17.7**
	v_{p_0}	0.07	0.10	0.14	0.06	0.09	0.12
	K_s	1.09	1.67	2.62	1.30	2.01	3.26
LA	E_{max}	0.35	0.38	0.42	0.78	0.78	0.77
	E_{min}	0.03	0.09	0.14	0.04	0.04	0.04
	m_1	0.02	0.08	0.12	0.04	0.09	0.13
	τ_1	0.02	0.07	0.10	0.03	0.03	0.03
	m_2	0.03	0.09	0.14	0.01	0.06	0.10
	τ_2	0.05	0.09	0.12	0.26	0.27	0.28
	v_{p_0}	0.07	0.09	0.14	0.03	0.03	0.03
	K_s	0.02	0.07	0.10	0.04	0.09	0.13
AV	A_{max}	0.55	0.78	1.10	**3.27**	**4.82**	**7.25**
	$\boldsymbol{A_{min}}$	**12.8**	**16.6**	**22.6**	-	-	-
	l	0.47	0.72	1.0	0.56	0.80	1.16
	K_{vo}	0.09	0.09	0.15	0.17	0.32	0.51
	K_{vc}	0.29	0.43	0.61	0.80	1.13	1.59
MV	A_{max}	0.09	0.12	0.15	4.09	4.09	4.02
	$\boldsymbol{A_{min}}$	**4.34**	**6.73**	**10.4**	-	-	-
	l	0.04	0.09	0.13	0.04	0.09	0.14
	K_{vo}	0.03	0.07	0.11	0.04	0.09	0.12
	K_{vc}	0.02	0.07	0.11	0.02	0.07	0.11